HHS Public Access

Author manuscript

Magn Reson Med. Author manuscript; available in PMC 2021 January 01.

Published in final edited form as:

Magn Reson Med. 2020 January ; 83(1): 94–108. doi:10.1002/mrm.27903.

GRASP-Pro: imProving GRASP DCE-MRI through self-calibrating subspace-modeling and contrast phase automation

Li Feng[1], **Qiuting Wen**[2], **Chenchan Huang**[3], **Angela Tong**[3], **Fang Liu**[4], **Hersh Chandarana**[3,5]

[1] Department of Medical Physics, Memorial Sloan Kettering Cancer Center, New York, NY, United States

[2] Department of Radiology and Imaging Sciences, Indiana University School of Medicine, Indianapolis, Indiana, United States

[3] Department of Radiology, New York University School of Medicine, New York, NY, United States

[4] Department of Radiology, University of Wisconsin-Madison, Madison, Wisconsin, United States

[5] Center for Advanced Imaging Innovation and Research (CAI^{2}R), New York University School of Medicine, New York, NY, United States

Abstract

Purpose—To propose a highly-accelerated, high-resolution dynamic contrast-enhanced MRI (DCE-MRI) technique called GRASP-Pro (Golden-angle RAdial Sparse Parallel imaging with imProved performance) through a joint sparsity and self-calibrating explicit subspace-constraint with automated selection of contrast phases.

Methods—GRASP-Pro reconstruction enforces a combination of self-calibrating explicit low-rank subspace-constraint and temporal sparsity constraint. The temporal basis used to construct subspace is estimated from an intermediate reconstruction using the low-resolution portion of radial k-space, which eliminates the need for generating the basis using auxiliary data or a physical signal model. A convolutional neural network was trained to generate the contrast enhancement curve in the artery, from which clinically-relevant contrast phases are automatically selected for evaluation. The performance of GRASP-Pro was demonstrated for high spatiotemporal resolution DCE-MRI of the prostate and was compared against standard GRASP in terms of overall image quality, image sharpness, and residual streaks/noise level.

Results—Compared to GRASP, GRASP-Pro was able to reconstruct dynamic images with enhanced sharpness, less residual streaks/noise and finer delineation of the prostate without prolonging reconstruction time. The image quality improvement reaches statistical significance (P<0.05) in all the assessment categories. The neural network successfully generated contrast enhancement curves in the artery, and corresponding peak enhancement indexes correlated well with that from the manual selection.

Address correspondence to: Li Feng, PhD, Department of Medical Physics, Memorial Sloan Kettering Cancer Center, 1250 1st Ave, New York, NY, USA 10065, lifeng.mri@gmail.com.

DISCLOSURE

Li Feng and Hersh Chandarana are co-inventors of a patent (Patent number 9921285) on the GRASP imaging technique.

Conclusion—GRASP-Pro is a promising method for rapid and continuous DCE-MRI. It enables superior reconstruction performance over standard GRASP and allows reliable generation of artery enhancement curve to guide the selection of desired contrast phases for improving the efficiency of GRASP MRI workflow.

Keywords

GRASP-Pro; Golden-Angle Radial; Subspace Modeling; Compressed Sensing; Rapid DCE-MRI

INTRODUCTION

The combination of compressed sensing with golden-angle radial imaging has gained substantial interest in recent years and has facilitated many imaging applications with encouraging clinical performance. On the one hand, the golden-angle radial rotation scheme (1) enables continuous and motion-robust data acquisitions, allows flexible data sorting and retrospective selection of temporal resolution, and can eliminate the need for breath holding (2–4). On the other hand, the inherent incoherent undersampling property of radial imaging can be explored in sparsity-based reconstruction to achieve highly-accelerated data acquisitions (5). With a synergistic combination of multicoil compressed sensing and golden-angle radial sampling, a continuous free-breathing imaging method called GRASP (Golden-angle Radial Sparse Parallel) MRI was developed (6), and it has been extensively evaluated in a variety of oncological imaging applications in a clinical environment (7).

After the initial development of GRASP, several novel approaches have been presented in connection with this imaging framework for improved performance. For example, a tiny golden-angle rotation scheme was designed to mitigate eddy current effects caused by large gradient jumps in standard golden-angle imaging (8), and it has demonstrated better image quality in several cardiac MRI studies (9–11). A method of reconstructing golden-angle radial images with extra motion dimensions, called XD-GRASP (GRASP imaging with eXtra Dimensions) (12), has been proposed as a new way of handling respiratory motion, with superior imaging performance to standard motion-averaged reconstruction (13). Such an imaging and reconstruction strategy is not limited to the management of motion and can also be explored to generate new information of potential clinical value (14,15), or to address other unwanted effects such as contrast blurring in 3D fast spin-echo MRI (16). In a more recent study, GRASP has also been extended to a further optimized framework called RACER-GRASP (Respiratory-weighted, Aortic Contrast Enhancement-guided and coil-unstReaking GRASP) (17) for improved dynamic contrast-enhanced MRI (DCE-MRI) of the liver, which enables contrast enhancement curve-guided data sorting, reduced motion blurring, and less residual streaking artifacts. Moreover, the self-calibrating GeneRalized autocalibrating partial parallel acquisition Operator Gridding (GROG), previously proposed as an alternative algorithm to standard gridding in non-Cartesian MRI reconstruction (18), has been combined with GRASP to eliminate the need of gridding and re-gridding during iterative reconstruction for faster reconstruction speed (19).

Despite past efforts for optimizing the GRASP framework, its reconstruction algorithm has largely remained the same since its initial development. In most situations, a first-order finite

differences operation is employed along the dynamic dimension as a temporal total variation (TV) constraint. As a result, the reconstruction quality of GRASP can be relatively poor at high acceleration rates. This is one of the main reasons why clinical GRASP images are currently reconstructed with a relatively low temporal resolution (e.g., 15–20 seconds/image volume) for qualitative multiphase evaluation only (7). Meanwhile, at high temporal resolutions, a reconstructed GRASP image-series can contain a large number of dynamic frames, making it difficult for radiologists to choose their desired contrast phases for clinical diagnosis. Therefore, additional developments are needed to further improve the acceleration capabilities and the overall pipeline of GRASP, which can provide better image quality at high acceleration rates with higher resolution and can optimize the usefulness of GRASP in clinical environment.

Inspired by many accelerated dynamic MRI studies with low-rank subspace modeling (16,20–34), the first contribution of this work was to optimize the GRASP framework with improved reconstruction performance through an additional explicit subspace constraint that is tailored to take advantage of the unique sampling geometry of radial imaging. Specifically, we aim to extend the previous subspace-constrained methods to incorporate a new self-calibrating subspace-constraint component and to combine this reconstruction framework with radial sampling. The temporal basis used to generate a subspace for enforcing an explicit low-rank constraint is directly estimated from undersampled radial data without using a physical signal model or acquiring additional training data. The second contribution of this work was to apply a convolutional neural network that is trained to guide the selection of clinically-relevant contrast phases based on an automatically generated contrast enhancement curve in the artery. In the following sections, existing subspace-constrained reconstruction methods are briefly summarized first, followed by the description of our proposed new method, called GRASP-Pro (GRASP MRI with imProved performance). The new method was then applied for high resolution DCE-MRI of the prostate and was compared to standard GRASP.

METHODS

Subspace-Constrained Dynamic Image Reconstruction: A Brief Summary of Existing Works

The low-rank model has been extensively studies in MRI reconstruction to exploit the strong spatiotemporal correlations in dynamic imaging for accelerated data acquisitions (35). Generally, there are different ways of exploiting the low-rank structure, for example, through an implicit low-rank constraint or an explicit low-rank constraint. An easy way to enforce implicit low-rank constraint is to use a nuclear norm that leads to a convex optimization problem (36). Other more advanced methods, such as the k-t SLR technique (37,38), can enforce an implicit low-rank constraint with a Schatten-norm (in a non-convex form) for better reconstruction performance, and the reconstruction enables joint recovery of low-rank model basis and model coefficients. Despite its increased flexibility and robustness in basis estimation, it has been shown that k-t SLR suffers from heavy computation burden and memory requirements (25), which poses challenges in clinical translation. An alternative way of exploiting the low-rank model is to enforce an explicit low-rank constraint in a so-

called subspace, based on the fact that a dynamic image series can be represented in a lower dimensional subspace if the corresponding temporal basis is pre-known. Compared to reconstruction enforcing an implicit low-rank constraint without generating subspace, explicit subspace modeling leads to reduced degrees of freedom and thus improved reconstruction performance, as well as greatly increased reconstruction speed (25,35). For example, a prior study showed that enforcing an explicit low-rank constraint can be more effective and more efficient compared to k-t SLR (25). This type of methods, referred to as explicit subspace-constraint, or explicit subspace-modeling, will be the primary focus for the subsequent discussion.

Based on the way of estimating the temporal basis, existing reconstruction techniques enforcing an explicit subspace low-rank constraint can roughly be divided into two categories, either model-driven subspace estimation or data-driven subspace estimation. For the model-driven approach, the temporal basis is typically estimated using a physical signal model. For example, a T_1 or T_2 relaxation model with additional B_1 and/or B_0 considerations can be used to generate an ensemble of possible signal curves covering a range of to-be-estimated parameters, from which a temporal basis can be generated using principal component analysis (PCA) or singular value decomposition (SVD). Several novel approaches belonging to this category have shown great promise in accelerated MR parameter mapping or MR fingerprinting (21,24,31,33) and contrast-resolved 3D FSE imaging (16). However, in certain dynamic imaging applications, such as cine imaging or DCE-MRI, a signal model may not be available, or it is not sufficient to accurately represent the temporal signal evolution. In this case, estimating the temporal basis from auxiliary training data that are acquired separately or within the low-resolution k-space region (referred to as the data-driven approach) can be more reliable. This type of methods has been demonstrated for cardiac MRI (25,26,32,39), MR spectroscopic imaging (MRSI) (27,30), speech imaging (29), MR parameter mapping (23,28) and DCE-MRI (22,34,39). Nevertheless, despite improved robustness in capturing underlying dynamics, these methods usually require acquisition of additional auxiliary data, or modification of sampling trajectories to incorporate a fully-sampled low-resolution region for estimating the basis, thus limiting achievable acceleration rates.

GRASP-Pro: Self-Calibrating Subspace-Constrained Reconstruction for Dynamic Radial MRI

Radial sampling offers a unique sampling geometry where the undersampling rate is much lower around the central k-space region, as shown in Figure 1a. Therefore, even at high acceleration rates, a low spatial resolution dynamic image-series can still be reliably reconstructed with conventional sparse reconstruction, such as standard GRASP. This reconstructed image-series, despite reduced spatial resolution, can still provide sufficient temporal information for estimating a temporal basis to represent the full-resolution image-series in a low-dimensional subspace (25). Figure 1b shows a representative fully sampled radial prostate image with corresponding down-sampled images at different spatial resolution/matrix size. Here, the full-resolution matrix size is denoted as NxN and the low-resolution matrix size is denoted as LxL. In this specific example representing our target application in this study, N=448 and L=128, 96, and 32. It can be observed that the general

image content can still be recognized down to a matrix size of 96×96. Figure 2a shows the gridding and GRASP reconstruction at a resolution of 96×96 with only 10 consecutive spokes in each dynamic frame (L=96). In this example, the number of dynamic frames, denoted as T, is 175. The low-resolution GRASP reconstruction using GROG (19) can be performed by solving:

$$\widetilde{m}_L = \arg\min_{m_L} \frac{1}{2}\|Em_L - \sqrt{W_L}y_L\|_2^2 + \lambda\left\|Sm_L\right\|_1 \quad [1]$$

Equation 1 aims to reconstruct a low-resolution dynamic image-series $m_L \in \mathbf{C}^{T\times L\hat{}2}$ (e.g., L=96, T=175) in which each row represents a concatenated dynamic image frame and each column represents the time dimension for a given pixel. y_L is the sorted low-resolution dynamic k-space shifted to a Cartesian grid using GROG, W_L is corresponding GROG weighting function for compensating varying sampling density (19). $E = \sqrt{W_L}FC$ is the encoding operator incorporating coil sensitivities (C) calculated at this resolution, Fourier transform (F) and the GROG weighting function (W_L). S represents the sparsifying transform and is selected as first-order finite differences along the dynamic dimension to minimize temporal TV in the image space with a regularization parameter λ. Low-resolution GRASP reconstruction successfully removed streaking artifacts with good temporal fidelity, as shown in Figure 2b comparing the normalized signal-time curves in the femoral artery (yellow arrow in the image) between GRASP and gridding reconstructions, Here, the signal-time curve from the gridding images is used as a reference to assess temporal fidelity, as recommended in the original GRASP study (6).

After the intermediate reconstruction step, an orthonormal basis can then be generated from the reconstructed low-resolution dynamic image-series using PCA:

$$m_L = UV_L \quad [2]$$

where $U \in \mathbf{C}^{T\times T}$ is the basis and $V_L \in \mathbf{C}^{T\times L\hat{}2}$ represents the associated coefficients to represent the low-resolution image-series under U. Corresponding singular values, shown in Figure 2c, indicate that the image-series has a low rank and can be represented by only the first K dominant basis components (e.g., 5 in the example according to the decaying pattern of singular values, referred to as principal components, or PCs) without losing important information (16,20), such that:

$$UV_L \approx U_K V_{LK} \quad [3]$$

where $U_K \in \mathbf{C}^{T\times K}$, $V_{LK} \in \mathbf{C}^{K\times L\hat{}2}$, and $K << T$. This preliminary investigation indicates that for radial imaging, a temporal basis can be obtained from the low-resolution k-space

following a standard GRASP reconstruction for subsequent subspace modeling, thus eliminating the need for a physical signal model or additional training data. This observation is further demonstrated in supporting Figure S1 (Supporting Information), where using a basis estimated from low-resolution GRASP images, an undersampled full-resolution image-series (a) can be compressed to a low-dimensional sparse subspace with only 4–5 PCs significant components (b).

Following the basis estimation, GRASP-Pro reconstruction can be performed by solving:

$$\tilde{V}_K = \arg\min_{V_K} \frac{1}{2}\|E(U_K V_K) - \sqrt{W}y\|_2^2 + \lambda\left\|S(U_K V_K)\right\|_1 \quad [4]$$

where y is the sorted full-resolution dynamic k-space shifted to a Cartesian grid using GROG and U_K is the pre-estimated basis with K PCs. Equation 4 aims to solve $V_K \in \mathbf{C}^{K \times N\text{^}2}$, the coefficients in subspace to represent the full-resolution image-series under U_K. Once V_K is reconstructed, the to-be-reconstructed fully-resolution dynamic images $m \in \mathbf{C}^{T \times N^2}$ can be computed as $U_K V_K$. Comparing Equation 4 with Equation 1, it can be seen that GRASP-Pro extends the standard GRASP reconstruction through an additional explicit self-calibrating subspace-constraint to exploit joint low-rank and temporal sparse structures, where the temporal basis is estimated from an intermediate GRASP reconstruction. A flowchart of the GRASP-Pro reconstruction is summarized in Figure 3.

Pre-Optimization of Reconstruction Protocol

It has been observed in Figure 1 that a matrix size of 96×96 can be a good option to perform the intermediate reconstruction for generating the basis. However, another two questions needed to be answered prior to implementing the GRASP-Pro reconstruction included: 1) what is a good number of K in Equation 4, and 2) can we estimate a temporal basis from low-resolution gridding images without running GRASP? This section addresses these questions by investigating the modeling error and compression power using compressed images generated from different pre-estimated basis on a sample undersampled radial DCE dataset (matrix size=448×448, voxel size=1.07×1.07mm^2, 175 frames, 10 connective spokes each frame). Here, compressed images are defined as full-resolution images generated from subspace by keeping only the first K dominant PCs. As an example, shown in supporting Figure S1 (Supporting Information), a dataset has a matrix size of 448×448×175 (a), and if only the first 5 dominant PCs are kept in the temporal basis, the original images can be transferred to a low-dimensional subspace with a size of 448×448×5 (b). The “compressed images” (448×448×175) is then generated from this reduced subspace using the same 5 PCs (c).

The Size of Subspace—In the first step, we investigated the influence of K on corresponding compressed images in three datasets. The normalized signal-time profile of the right femoral artery (yellow arrow in Figure 4) was used for validating temporal fidelity, because contrast enhancement in the artery has a sharp signal uptake that can be used to test

a reconstruction task. The gridding images, despite streaking artifacts, still represented the true underlying temporal evolution and was thus used as a comparison reference (6). The temporal basis was estimated from a low-resolution GRASP reconstruction with a matrix size of 96×96. As seen in Figure 4 for one example, a small number of PCs (e.g., 2 PCs) presented clean image appearances but failed to produce an accurate temporal profile, while too many PCs (e.g., 16 PCs) led to residual streaking artifacts as seen from the temporal profile. 5 PCs was found to provide a good performance between the compression power and the modeling error, and this finding correlated well with the observation of the singular value decay in Figure 2c. It was further confirmed that 5 PCs were able to represent the low-resolution GRASP images with a root mean square error (RMSE) lower than 0.2% in the three testing datasets.

Is the Intermediate GRASP Reconstruction Necessary?—In the second step, we examined the influence of temporal basis estimated from both GRASP reconstruction and gridding reconstruction with a matrix size of 96×96, referred to as Sub 96-GRASP and Sub 96-Gridding, respectively. The dominant 5 PCs were kept in the temporal basis for generating compressed images for both reconstructions. Compared with Sub 96-GRASP, Sub 96-Gridding failed to maintain temporal fidelity and showed noted streaking artifacts in the compressed images, as shown in Figure 5. Moreover, we further evaluated compressed images using a basis estimated from a low-resolution gridding reconstruction with a matrix size of 6×6, referred to as Sub 6-Gridding. Here, 10 spokes satisfy the Nyquist sampling rate (40) and thus are considered as fully sampling for a 6×6 image. Sub 6-Gridding showed even worse performance, potentially due to substantial loss of image information at such a low spatial resolution. These preliminary results validated that the intermediate low-resolution GRASP reconstruction is an essential step for generating accurate temporal basis in the proposed GRASP-Pro reconstruction.

Datasets

This study was approved by IRB and was HIPAA-compliant. MR raw data from twenty-two male patients were retrospectively collected, and written informed consent was waived per IRB approval. Each dataset was acquired on a clinical 3T MR scanner (MAGNETOM Prisma, Siemens Healthineers, Germany) in transverse orientation using a prototype fat-saturated 3D stack-of-stars golden-angle radial imaging sequence. Imaging parameters included: TR/TE = 4.12/1.96 ms, matrix size = 224×224×(21–26), in-plane field of view (FOV) = 240×240 mm^2, voxel size = 1.07×1.07×3.0 mm^3, flip angle = 12°. 1755 spokes were acquired for each partition, and the average scan time was 197.45 ± 12.51 seconds. A full-dose of contrast agent (Gadavist, Bayer Healthcare) was injected at a rate of 2 ml/sec.

Image Reconstruction

For each dataset, k-space were first compressed to 8 virtual channels (41) and GROG was then performed to shift the radial data onto a Cartesian grid for subsequent iterative reconstruction (19). Coil sensitivity maps were estimated from a static 3D image volume reconstructed using all the acquired spokes using the adaptive combination approach (42). Both standard GRASP and GRASP-Pro reconstructions were performed after grouping 10 consecutive spokes into one dynamic frame, resulting in a temporal resolution of ~1–1.2

seconds/volume. Following the previously optimized protocol, the temporal basis used in GRASP-Pro was estimated from an intermediate low-resolution (96×96) GRASP reconstruction and the first 5 PCs were used to construct the subspace. The regularization parameter was empirically selected by a body radiologist (H.C.) with 11 years post-fellowship clinical experience. Specifically, the radiologist compared reconstructed images series with a range of regularization weights in three datasets, and the value that achieved the best visual balance between the image quality and temporal fidelity was selected as the regularization parameter. Here, the temporal fidelity was assessed in a region of interest (ROI) placed on the femoral artery and was assessed using gridding images as a reference, as described in (6). The parameter was selected separately for GRASP and GRASP-Pro and was fixed for all the datasets. All the reconstructions were implemented in MATLAB (Mathworks, MA) in a server equipped with 512 GB RAM and one 24-GB NVIDIA GPU card using a non-linear conjugate gradient algorithm, and the number of iterations (a total of 24 iterations, including 3 out loops and 8 inner iterations each) was set the same for GRASP and GRASP-Pro. To speed up the computational process, the iterative reconstruction was performed in GPU using the MATLAB function “gpuArray” and the reconstruction was performed slice by slice.

Learning-Based Contrast Phase Selection

Deep learning was used to provide automatic detection of artery regions in the reconstructed images, from which an artery contrast enhancement curve can be obtained to guide the selection of desired contrast phases for clinical use. Specifically, a convolutional encoder-decoder (CED) network (43) (supporting Figure S2, Supporting Information), previously shown for accurate and efficient multi-tissue segmentation (43–45), was trained to segment the femoral arteries in the prostate images. The images and segmentation masks used for training were obtained on 7 additional prostate datasets (different from the 22 data used for image reconstruction, with IRB approval for waived written informed consent) acquired with the same protocol. The 7 datasets were reconstructed as 3D static volumes combining all the acquired spokes, and the training was performed using the central 12 slices containing both the right and left femoral arteries. Manual labeling of the femoral arteries was performed by an observer (Q.W.) with 10 years of imaging research experience. The network training was performed using a multiple-class cross-entry loss and using a Stochastic Gradient Descent (SGD) algorithm with a learning rate of 0.01 and a total of 50 epochs for ensuring training convergence. The trained network was then applied to automatically segment both the right and left femoral arteries on a delayed phase from the GRASP-Pro reconstruction. After segmenting the arteries, an ensemble of contrast enhancement curves, each from one detected artery ROI, were generated for each dataset. A clustering algorithm, as described in (17) for details, was applied to generate a single artery contrast enhancement curve from the ensemble. Based on this contrast curve and the corresponding peak artery enhancement index, one pre-contrast phase (30 seconds before the peak artery enhancement), one early-arterial phase (15 seconds after the peak artery enhancement), one late-arterial phases (45 seconds after the peak artery enhancement) and one delayed phase (90 seconds after the peak artery enhancement) were automatically selected.

Image Evaluation

The automatically selected dynamic phases (44 pre-contrast phase images, 88 early and late arterial phase images and 44 delayed phase images) from both the GRASP and GRASP-Pro results were randomized and pooled together for visual image quality assessment. Two board-certified abdominal radiologists (C.H. and A.T., with 3 years and 1 year of post-fellowship clinical experience, respectively), who were blinded to the reconstruction schemes, scored the overall image quality, the sharpness of prostatic capsule and the overall streaking artifact/noise level of each case. A 4-point Likert-type scale was used for the scoring (46): overall image quality: 4=good, 3=adequate, 2=borderline, 1=non-diagnostic; sharpness of prostatic capsule: 4=good, 3=adequate, 2=partially seen, 1=not seen; overall artifact/noise level: 4=none, 3=mild, 2=significant, 1= unreadable. The reported scores were averaged over the two readers and were represented by the mean ± standard deviation. A non-parametric paired two-tailed Wilcoxon signed-rank test was performed for statistical assessment, with a *P*-value less than 0.05 indicating statistical significance.

To evaluate the accuracy of the automatic artery segmentation, the femoral arteries on all the 22 prostate datasets were also manually segmented (the central 12 slices). The dynamic time point/index where the artery contrast enhancement reaches its peak was obtained from both the manually-generated curves and the automatically-generated curves for each dataset. Linear regression was used to assess the correlation between the manually-identified and automatically-identified peak indexes. Note that the purpose of generating artery enhancement curve is to identify its peak enhancement position mimicking the bolus timing in clinical DCE-MRI, so that clinically-relevant contrast phases can be automatically selected as described above.

RESULTS

The mean reconstruction time for GRASP and GRASP-Pro was 30.79±2.30 minutes and 30.33±2.38 minutes, respectively. Figure 6a shows a prostate case comparing gridding images, compressed images with 5 PCs and GRASP-Pro. The compressed images already have fewer streaking artifacts than gridding images but suffer from image blurring and residual streaks (yellow arrow), GRASP-Pro further refined image details with improved delineation of the prostate, muscle and small vessels. Figure 6b shows normalized signal-time curves from the right femoral artery, suggesting good temporal fidelity of the GRASP-Pro reconstruction with respect to the gridding reference.

Figure 7 and Figure 8 show the comparison of GRASP with GRASP-Pro in two prostate cases, together with corresponding normalized signal-time curves in the right femoral artery and an ROI inside the prostate (red circle). Compared to standard GRASP reconstruction, GRASP-Pro produced similar temporal behavior but achieved enhanced image sharpness (yellow arrows), less noise/artifacts (green arrows), and better overall delineation of the prostate tissue in different contrast phases. The comparison of GRASP and GRASP-Pro in two additional patients is shown in supporting Figure S3 (Supporting Information), where GRASP-Pro shows similar improvement in image quality over standard GRASP. The visual image quality scores averaged from all the patient datasets over the two readers are summarized in Table 1. While GRASP yielded adequate image quality in different contrast

phases (average score around 3), GRASP-Pro achieved further improved overall image quality, the sharpness of the prostate and less streaks/noise (average score around 3.9), with statistical significance ($P<0.05$) reached in all the assessment categories.

Figure 9a compares the automatic selection and manual selection of the right femoral arteries in three prostate cases. The trained CED network was able to successfully identify the arteries, so that a contrast enhancement curve can be automatically generated to guide the selection of desired contrast phases. Figure 9b shows the plot of linear correlation between the peak enhancement indexes obtained from the automatically-generated and manually-generated contrast enhancement curves, with an R-square of 0.996 indicating an excellent correlation between the manual selection and the deep learning-based automatic phase selection.

Supporting Figure S4 (Supporting Information) assesses the influence of varying regularization parameter λ on GRASP-Pro reconstruction. Specifically, we tested whether the temporal sparsity constraint is needed in GRASP-Pro by setting the parameter as zero. As can be seen from the supporting figure, GRASP-Pro reconstruction without temporal TV constraint ($\lambda=0$) suffered from residual noise, particularly in the arterial phase. On the other side, a high λ generated temporal blurring due to over-regularization as in standard compressed sensing reconstruction.

Supporting Figure S5 (Supporting Information) compares a delayed contrast phase from GRASP-Pro reconstruction (175 dynamic frames) with 5 PCs, 16 PCs and 175 PCs. Here, subspace is not generated if all the 175 PCs are kept for reconstruction. The results suggest that GRASP-Pro with 5 PCs achieved the best image quality among the three reconstructions. GRASP-Pro with 16 PCs suffered from certain loss of fine details as indicated by the yellow arrow. Without an explicit subspace constraint, GRASP-Pro with 175 PCs suffered from poorer overall image quality, image sharpness and the delineation of the prostate tissue.

Supporting Figure S6 (Supporting Information) compares four GRASP-Pro reconstructions in which the matrix size for the intermediate low-resolution GRASP reconstruction was set as 6, 32, 96 and 128, indicated as GRASP-Pro Sub 6 to Sub 128. It can be seen that GRASP-Pro Sub 128 achieved comparable image quality and temporal behavior compared to GRASP-Pro Sub 96. GRASP-Pro Sub 6 failed to reconstruct temporal information correctly and GRASP-Pro Sub 32 suffered from certain fluctuation in temporal signal profile. Overall, GRASP-Pro Sub 96 achieved a good balance between computation burden and reconstruction performance.

DISCUSSION

In this work, we presented a new rapid dynamic radial imaging approach called GRASP-Pro, which enables high spatiotemporal resolution DCE-MRI. Compared to the original GRASP technique, GRASP-Pro incorporates an additional self-calibrating explicit subspace constraint to achieve improved reconstruction performance. Different from MR parameter mapping or MR fingerprinting that can rely on Bloch equations to represent the signal

evolution correctly, the pharmacokinetic model in DCE-MRI has many uncertainties, and the development of more robust and accurate models for perfusion MRI is still an open question (47). Therefore, it can be more reliable to estimate a basis from the acquired data itself for subsequent subspace representation. Compared to prior subspace-based reconstruction approaches, the construction of subspace in GRASP-Pro takes advantage of the unique sampling geometry of radial imaging, which estimates a temporal basis from an intermediate iterative reconstruction performed on the central radial k-space, thus eliminating the need for a physical signal model or additional training data that may require extra scan time and may limit acceleration capabilities. As a result, the capture of underlying dynamics is more reliable and there is no need to modify existing sampling trajectories to acquire extra auxiliary data. Given that GRASP has already been translated for routine clinical use (48), the improved image quality provided by GRASP-Pro could achieve a better clinical impact, representing a valuable step to further improve the utility and usefulness of GRASP in diagnostic care. In addition, the incorporation of a convolutional neural network can improve the overall efficiency of current clinical GRASP workflow, making GRASP-Pro an optimized solution for rapid DCE-MRI.

Methods for estimating temporal basis from acquired data have been reported before. For example, k-t SLR (37,38) aims to jointly estimate a temporal basis with spectral regularization and reconstruct undersampled dynamic images exploiting low-rank and sparsity structures. Thus, it does not require additional training data or signal model for estimating a temporal basis and does not require the selection of low-resolution matrix size as in GRASP-Pro. However, there are a few key distinctions between k-t SLR and GRASP-Pro. First, k-t SLR enforces a low-rank constraint implicitly through the nuclear norm or Schatten-norm without generating a subspace, while GRASP-Pro enforces a low-rank constraint explicitly through the construction of a low-dimensional subspace. As described and validated in (25), enforcing a low-rank subspace-constraint explicitly has advantages in both imaging performance and computational efficiency. Specifically, the explicit constraint with subspace modeling (as in GRASP-Pro) has fewer degrees of freedom than the implicit constraint (as in k-t SLR), and thus the low-rank structure can be enforced more strongly to achieve better reconstruction quality (25). In addition, GRASP-Pro uses an intermediate step to pre-estimat temporal subspace, leading to reduced computational burden without performing the computation-intensive singular value decomposition (SVD) operation during the reconstruction process, thus enabling much faster reconstruction speed than k-t SLR. Moreover, k-t SLR requires selection of two regularization parameters for the implicit low-rank constraint and the sparsity constraint, respectively. GRASP-Pro, on the other hand, requires only one regularization parameter, making the selection process and the implementation easier.

A proper selection of the number of PCs is important to balance compression power, modeling error and sensitivity to noise (16,25,39) in GRASP-Pro and other subspace-constraint reconstruction methods. Insufficient basis components can yield temporal blurring (Figure 4), while excessive basis components may introduce residual noise/artifacts (supporting Figure S5, supporting information). Similar to prior subspace-based reconstruction studies, the number of PCs in this work (K=5) was empirically selected based

on **i)** the observation of the decaying pattern of singular value (Figure 2c) and **ii)** further evaluation on the so-called compressed images to assess temporal fidelity as shown in Figure 4. It is understandable and expected that this parameter will need to be re-selected for other types of applications where the underlying dynamics are different. As pointed out in (25), current subspace-based reconstruction methods typically rely on empirical selection of this parameter, and it is still an open question on how to automate this process across different applications with different underlying dynamics. However, a joint subspace low-rank and sparsity constraint can achieve improved robustness to the choice of this parameter (25).

In this study, we confirmed that the intermediate GRASP reconstruction is necessary for GRASP-Pro (Figure 5), and this does not prolong overall reconstruction time due to reduced matrix size in the intermediate reconstruction step. This reconstruction strategy can be particularly useful given the fact that at high acceleration rates, it is challenging to acquire a fully sampled low-resolution k-space region for estimating a temporal basis. The matrix size for the intermediate GRASP reconstruction was visually selected as 96×96 in this study to balance reconstruction quality and computational burden. A smaller matrix size may lead to suboptimal estimation of temporal basis and thus poor representation of the full-resolution images with the estimated basis (supporting Figure S6, supporting information). On the other hand, a larger matrix size prolongs overall reconstruction time and the performance of the intermediate GRASP reconstruction may be reduced due to higher undersampling factor.

A temporal TV constraint has been found to be effective in reconstructing undersampled dynamic images (49) and it has been routinely performed in standard GRASP reconstruction. Since images are already constrained to a low-dimensional subspace with low-rank modeling in GRASP-Pro, we assessed whether the additional TV constraint is necessary. From supporting Figure S4 (Supporting Information), it was found that although the TV constraint in GRASP-Pro has less influence in delayed phases, it indeed suppresses more artifacts/noise in the arterial phase, where the baseline signal-to-noise ratio (SNR) is relatively lower. It should be noted that the arterial phase is usually the most important part in DCE-MRI and thus this improvement is clinically significant. This finding also correlates well with prior observations in other studies, in which a combination of low-rank and sparsity constraints achieved better performance than either of them alone (28). However, as in other constrained reconstruction approaches, the use of temporal sparsity constraint requires selection of a regularization weight and this parameter is expected to be re-selected for different applications.

In GRASP-Pro, a neural network was trained to identify the arteries in the images, from which an artery enhancement curve can be automatically generated to guide the selection of desired contrast phases for clinical use based on the peak artery enhancement index. This component would be necessary in improving the efficiency of routine clinical workflow, given that over 100 dynamic frames can be generated in GRASP-Pro (e.g., 175 frames in this study) and thus manual selection of desired contrast phases (e.g., an arterial phase) can be cumbersome and time-consuming. Moreover, the deep learning-based artery selection does not rely on specific contrast enhancement pattern (17). As a result, this will be useful in DCE-MRI irrespective of contrast agent, dose, and volume, such as hepatobiliary contrast

agents Eovist that does not have a quick and sharp first pass dynamics. More importantly, the automatic segmentation of the artery could also be used to guide the generation of an arterial input function (AIF), which may facilitate automated perfusion image analysis, as shown in (50) for some preliminary results.

In this study, the GRASP-Pro has been demonstrated for DCE-MRI of the prostate where motion is generally not a major problem. The technique can be applied to other static organs such as the brain, neck or breast. However, the application of GRASP-Pro to moving organs, such as the liver or the lung, will require further optimization, given that respiratory motion is patient-dependent and thus the optimal number of PCs (K) needed in GRASP-Pro may vary from patient to patient. The motion management strategies proposed in the XD-GRASP (12) and RACER-GRASP (17) techniques could be further incorporated into GRASP-Pro to handle respiratory motion, but this will require additional investigation and will be explored in future work.

There are a few limitations in this study that warrant discussion. First, we did not compare different sparsity constraints. This was because a temporal TV constraint has been optimized and has been shown as an effective sparsity constraint in standard GRASP; and thus, for a fair comparison, we kept it identical in GRASP-Pro. Second, since an intermediate GRASP reconstruction is needed to generate a temporal basis, the maximum acceleration rate in GRASP-Pro can be limited by this reconstruction setting in order to ensure good reconstruction results in the intermediate step. In this work, 10 spokes per frame was empirically selected to allow a good fit into the available GPU memory, and reconstruction with a temporal resolution up to ~1 second per volume was demonstrated. Third, due to the limited number of datasets, our deep learning network for identifying the femoral arteries was trained on seven additional cases only. As can be seen from Figure 9, the performance of automatic segmentation of the artery varies from case to case. However, since the purpose of artery segmentation is only to obtain the peak artery enhancement timing, or the dynamic frame index, so that clinically relevant contrast phases can be selected automatically, a perfect segmentation of the artery with a high-level of precision is not required. Besides, we have applied a clustering algorithm (17) to further ensure the accuracy of generating contrast enhancement curves in the artery. Fourth, the GRASP-Pro reconstruction was performed slice by slice due to limited GPU memory. Additional optimization, such as parallelization of the reconstruction algorithm, will be important to further reduce reconstruction time for the translation of GRASP-Pro into the clinic.

CONCLUSION

GRASP-Pro has been shown as a promising tool for rapid and continuous DCE-MRI. Through the combination of a self-calibrating explicit subspace constraint and a temporal sparsity constraint, GRASP-Pro further pushes the acceleration rate and temporal resolution beyond what standard GRASP can achieve. GRASP-Pro also enables automatic selection of desired contrast phases that are clinically-relevant, and thus it is expected to further improve the overall efficiency and the clinical utility of GRASP in oncological applications.

Supplementary Material

Refer to Web version on PubMed Central for supplementary material.

ACKNOWLEDGEMENTS

This work was performed in part under the rubric of the Center for Advanced Imaging Innovation and Research (CAI^2R), a NIBIB Biomedical Technology Resource Center. Li Feng thanks Dr. Sajan Goud Lingala from the University of Iowa for helpful discussion.

REFERENCE

1. Winkelmann S, Schaeffter T, Koehler T, Eggers H, Doessel O. An optimal radial profile order based on the Golden Ratio for time-resolved MRI. IEEE Trans Med Imaging 2007;26(1):68–76. [PubMed: 17243585]
2. Chandarana H, Block TK, Rosenkrantz AB, Lim RP, Kim D, Mossa DJ, Babb JS, Kiefer B, Lee VS. Free-breathing radial 3D fat-suppressed T1-weighted gradient echo sequence: a viable alternative for contrast-enhanced liver imaging in patients unable to suspend respiration. Investigative radiology 2011;46(10):648–653. [PubMed: 21577119]
3. Chandarana H, Feng L, Block TK, Rosenkrantz AB, Lim RP, Babb JS, Sodickson DK, Otazo R. Free-breathing contrast-enhanced multiphase MRI of the liver using a combination of compressed sensing, parallel imaging, and golden-angle radial sampling. Investigative radiology 2013;48(1):10–16. [PubMed: 23192165]
4. Chandarana H, Block KT, Winfeld MJ, Lala SV, Mazori D, Giuffrida E, Babb JS, Milla SS. Free-breathing contrast-enhanced T1-weighted gradient-echo imaging with radial k-space sampling for paediatric abdominopelvic MRI. European radiology 2014;24(2):320–326. [PubMed: 24220754]
5. Lustig M, Donoho DL, Santos JM, Pauly JM. Compressed sensing MRI. Ieee Signal Proc Mag 2008;25(2):72–82.
6. Feng L, Grimm R, Block KT, Chandarana H, Kim S, Xu J, Axel L, Sodickson DK, Otazo R. Golden-angle radial sparse parallel MRI: combination of compressed sensing, parallel imaging, and golden-angle radial sampling for fast and flexible dynamic volumetric MRI. Magn Reson Med 2014;72(3):707–717. [PubMed: 24142845]
7. Feng L, Benkert T, Block KT, Sodickson DK, Otazo R, Chandarana H. Compressed sensing for body MRI. Journal of magnetic resonance imaging : JMRI 2017;45(4):966–987. [PubMed: 27981664]
8. Wundrak S, Paul J, Ulrici J, Hell E, Rasche V. A Small Surrogate for the Golden Angle in Time-Resolved Radial MRI Based on Generalized Fibonacci Sequences. Ieee T Med Imaging 2015;34(6):1262–1269.
9. Wundrak S, Paul J, Ulrici J, Hell E, Geibel MA, Bernhardt P, Rottbauer W, Rasche V. Golden ratio sparse MRI using tiny golden angles. Magn Reson Med 2016;75(6):2372–2378. [PubMed: 26148753]
10. Haris K, Hedstrom E, Bidhult S, Testud F, Maglaveras N, Heiberg E, Hansson SR, Arheden H, Aletras AH. Self-gated fetal cardiac MRI with tiny golden angle iGRASP: A feasibility study. Journal of magnetic resonance imaging : JMRI 2017;46(1):207–217. [PubMed: 28152243]
11. Haji-Valizadeh H, Rahsepar AA, Collins JD, Bassett E, Isakova T, Block T, Adluru G, DiBella EVR, Lee DC, Carr JC, Kim D, Binders CKDOMw, Nicotinamid ESG. Validation of highly accelerated real-time cardiac cine MRI with radial k-space sampling and compressed sensing in patients at 1.5T and 3T. Magn Reson Med 2018;79(5):2745–2751. [PubMed: 28921631]
12. Feng L, Axel L, Chandarana H, Block KT, Sodickson DK, Otazo R. XD-GRASP: Golden-angle radial MRI with reconstruction of extra motion-state dimensions using compressed sensing. Magn Reson Med 2016;75(2):775–788. [PubMed: 25809847]
13. Chandarana H, Feng L, Ream J, Wang A, Babb JS, Block KT, Sodickson DK, Otazo R. Respiratory Motion-Resolved Compressed Sensing Reconstruction of Free-Breathing Radial

Acquisition for Dynamic Liver Magnetic Resonance Imaging. Investigative radiology 2015;50(11):749–756. [PubMed: 26146869]

14. Cheng JY, Zhang T, Alley MT, Uecker M, Lustig M, Pauly JM, Vasanawala SS. Comprehensive Multi-Dimensional MRI for the Simultaneous Assessment of Cardiopulmonary Anatomy and Physiology. Sci Rep 2017;7(1):5330. [PubMed: 28706270]
15. Feng L, Delacoste J, Smith D, Weissbrot J, Flagg E, Moore WH, Girvin F, Raad R, Bhattacharji P, Stoffel D, Piccini D, Stuber M, Sodickson DK, Otazo R, Chandarana H. Simultaneous Evaluation of Lung Anatomy and Ventilation Using 4D Respiratory-Motion-Resolved Ultrashort Echo Time Sparse MRI. Journal of magnetic resonance imaging : JMRI 2019;49(2):411–422. [PubMed: 30252989]
16. Tamir JI, Uecker M, Chen W, Lai P, Alley MT, Vasanawala SS, Lustig M. T2 shuffling: Sharp, multicontrast, volumetric fast spin-echo imaging. Magn Reson Med 2017;77(1):180–195. [PubMed: 26786745]
17. Feng L, Huang C, Shanbhogue K, Sodickson DK, Chandarana H, Otazo R. RACER-GRASP: Respiratory-weighted, aortic contrast enhancement-guided and coil-unstreaking golden-angle radial sparse MRI. Magnetic resonance in medicine 2018;80(1):77–89. [PubMed: 29193260]
18. Seiberlich N, Breuer F, Blaimer M, Jakob P, Griswold M. Self-calibrating GRAPPA operator gridding for radial and spiral trajectories. Magn Reson Med 2008;59(4):930–935. [PubMed: 18383296]
19. Benkert T, Tian Y, Huang C, DiBella EVR, Chandarana H, Feng L. Optimization and validation of accelerated golden-angle radial sparse MRI reconstruction with self-calibrating GRAPPA operator gridding. Magn Reson Med 2018;80(1):286–293. [PubMed: 29193380]
20. Pedersen H, Kozerke S, Ringgaard S, Nehrke K, Kim WY. k-t PCA: temporally constrained k-t BLAST reconstruction using principal component analysis. Magn Reson Med 2009;62(3):706–716. [PubMed: 19585603]
21. Doneva M, Bornert P, Eggers H, Stehning C, Senegas J, Mertins A. Compressed sensing reconstruction for magnetic resonance parameter mapping. Magn Reson Med 2010;64(4):1114–1120. [PubMed: 20564599]
22. Brinegar C, Schmitter SS, Mistry NN, Johnson GA, Liang ZP. Improving temporal resolution of pulmonary perfusion imaging in rats using the partially separable functions model. Magn Reson Med 2010;64(4):1162–1170. [PubMed: 20564601]
23. Petzschner FH, Ponce IP, Blaimer M, Jakob PM, Breuer FA. Fast MR parameter mapping using k-t principal component analysis. Magn Reson Med 2011;66(3):706–716. [PubMed: 21394772]
24. Huang C, Graff CG, Clarkson EW, Bilgin A, Altbach MI. T2 mapping from highly undersampled data by reconstruction of principal component coefficient maps using compressed sensing. Magn Reson Med 2012;67(5):1355–1366. [PubMed: 22190358]
25. Zhao B, Haldar JP, Christodoulou AG, Liang ZP. Image Reconstruction From Highly Undersampled (k, t)-Space Data With Joint Partial Separability and Sparsity Constraints. Ieee T Med Imaging 2012;31(9):1809–1820.
26. Christodoulou AG, Zhang HS, Zhao B, Hitchens TK, Ho C, Liang ZP. High-Resolution Cardiovascular MRI by Integrating Parallel Imaging With Low-Rank and Sparse Modeling. Ieee T Bio-Med Eng 2013;60(11):3083–3092.
27. Lam F, Liang ZP. A subspace approach to high-resolution spectroscopic imaging. Magn Reson Med 2014;71(4):1349–1357. [PubMed: 24496655]
28. Zhao B, Lu W, Hitchens TK, Lam F, Ho C, Liang ZP. Accelerated MR parameter mapping with low-rank and sparsity constraints. Magn Reson Med 2015;74(2):489–498. [PubMed: 25163720]
29. Fu M, Zhao B, Carignan C, Shosted RK, Perry JL, Kuehn DP, Liang ZP, Sutton BP. High-resolution dynamic speech imaging with joint low-rank and sparsity constraints. Magn Reson Med 2015;73(5):1820–1832. [PubMed: 24912452]
30. Ma C, Clifford B, Liu Y, Gu Y, Lam F, Yu X, Liang ZP. High-resolution dynamic (31) P-MRSI using a low-rank tensor model. Magn Reson Med 2017;78(2):419–428. [PubMed: 28556373]
31. Asslander J, Cloos MA, Knoll F, Sodickson DK, Hennig J, Lattanzi R. Low rank alternating direction method of multipliers reconstruction for MR fingerprinting. Magn Reson Med 2018;79(1):83–96. [PubMed: 28261851]

32. Christodoulou AG, Shaw JL, Nguyen C, Yang Q, Xie YB, Wang N, Li DB. Magnetic resonance multitasking for motion-resolved quantitative cardiovascular imaging. Nat Biomed Eng 2018;2(4): 215–226. [PubMed: 30237910]
33. Zhao B, Setsompop K, Adalsteinsson E, Gagoski B, Ye H, Ma D, Jiang Y, Ellen Grant P, Griswold MA, Wald LL. Improved magnetic resonance fingerprinting reconstruction with low-rank and subspace modeling. Magn Reson Med 2018;79(2):933–942. [PubMed: 28411394]
34. Wang N, Christodoulou AG, Xie Y, Wang Z, Deng Z, Zhou B, Lee S, Fan Z, Chang H, Yu W, Li D. Quantitative 3D dynamic contrast-enhanced (DCE) MR imaging of carotid vessel wall by fast T1 mapping using Multitasking. Magn Reson Med 2019;81(4):2302–2314. [PubMed: 30368891]
35. Liang ZP. Spatiotemporal imaging with partially separable functions. 2007 4th Ieee International Symposium on Biomedical Imaging : Macro to Nano, Vols 1–3 2007:988–991.
36. Zhang T, Pauly JM, Levesque IR. Accelerating parameter mapping with a locally low rank constraint. Magn Reson Med 2015;73(2):655–661. [PubMed: 24500817]
37. Lingala SG, Hu Y, DiBella E, Jacob M. Accelerated Dynamic MRI Exploiting Sparsity and Low-Rank Structure: k-t SLR. Ieee T Med Imaging 2011;30(5):1042–1054.
38. Lingala SG, DiBella E, Adluru G, McGann C, Jacob M. Accelerating free breathing myocardial perfusion MRI using multi coil radial k - t SLR. Physics in Medicine and Biology 2013;58(20): 7309–7327. [PubMed: 24077063]
39. Velikina JV, Samsonov AA. Reconstruction of dynamic image series from undersampled MRI data using data-driven model consistency condition (MOCCO). Magn Reson Med 2015;74(5):1279–1290. [PubMed: 25399724]
40. Block KT. Advanced methods for radial data sampling in magnetic resonance imaging. PhD Disseration, University of Goettingen, 2008.
41. Huang F, Vijayakumar S, Li Y, Hertel S, Duensing GR. A software channel compression technique for faster reconstruction with many channels. Magnetic resonance imaging 2008;26(1):133–141. [PubMed: 17573223]
42. Walsh DO, Gmitro AF, Marcellin MW. Adaptive reconstruction of phased array MR imagery. Magn Reson Med 2000;43(5):682–690. [PubMed: 10800033]
43. Liu F, Zhou Z, Jang H, Samsonov A, Zhao G, Kijowski R. Deep convolutional neural network and 3D deformable approach for tissue segmentation in musculoskeletal magnetic resonance imaging. Magn Reson Med 2018;79(4):2379–2391. [PubMed: 28733975]
44. Liu F, Jang H, Kijowski R, Bradshaw T, McMillan AB. Deep Learning MR Imaging-based Attenuation Correction for PET/MR Imaging. Radiology 2018;286(2):676–684. [PubMed: 28925823]
45. Zhou Z, Zhao G, Kijowski R, Liu F. Deep convolutional neural network for segmentation of knee joint anatomy. Magn Reson Med 2018;80(6):2759–2770. [PubMed: 29774599]
46. Dickinson L, Ahmed HU, Allen C, Barentsz JO, Carey B, Futterer JJ, Heijmink SW, Hoskin P, Kirkham AP, Padhani AR, Persad R, Puech P, Punwani S, Sohaib A, Tombal B, Villers A, Emberton M. Scoring systems used for the interpretation and reporting of multiparametric MRI for prostate cancer detection, localization, and characterization: could standardization lead to improved utilization of imaging within the diagnostic pathway? Journal of magnetic resonance imaging : JMRI 2013;37(1):48–58. [PubMed: 22566285]
47. Essig M, Shiroishi MS, Nguyen TB, Saake M, Provenzale JM, Enterline D, Anzalone N, Dorfler A, Rovira A, Wintermark M, Law M. Perfusion MRI: The Five Most Frequently Asked Technical Questions. Am J Roentgenol 2013;200(1):24–34. [PubMed: 23255738]
48. Block KT, Grimm G, Feng L, Otazo R, Chandarana H, Bruno M, Geppert C, Sodickson DK. Bringing Compressed Sensing to Clinical Reality: Prototypic Setup for Evaluation in Routine Applications. In Proceedings of the 21st Annual Meeting of ISMRM, Salt Lake City, 2013 p. 3809.
49. Feng L, Srichai MB, Lim RP, Harrison A, King W, Adluru G, Dibella EV, Sodickson DK, Otazo R, Kim D. Highly accelerated real-time cardiac cine MRI using k-t SPARSE-SENSE. Magn Reson Med 2013;70(1):64–74. [PubMed: 22887290]
50. Feng L, Liu F, Rusinek H, Dane B, Brody H, Chitiboi T, Sodickson D, Otazo R, Chandarana H. AUTO-DCE-MRI: A Deep-Learning Augmented Liver Imaging Framework for Fully-Automated

Multiphase Assessment and Perfusion Mapping. Proceedings of the 26th Annual Meeting of ISMRM, Paris, France, 2018 p3481.

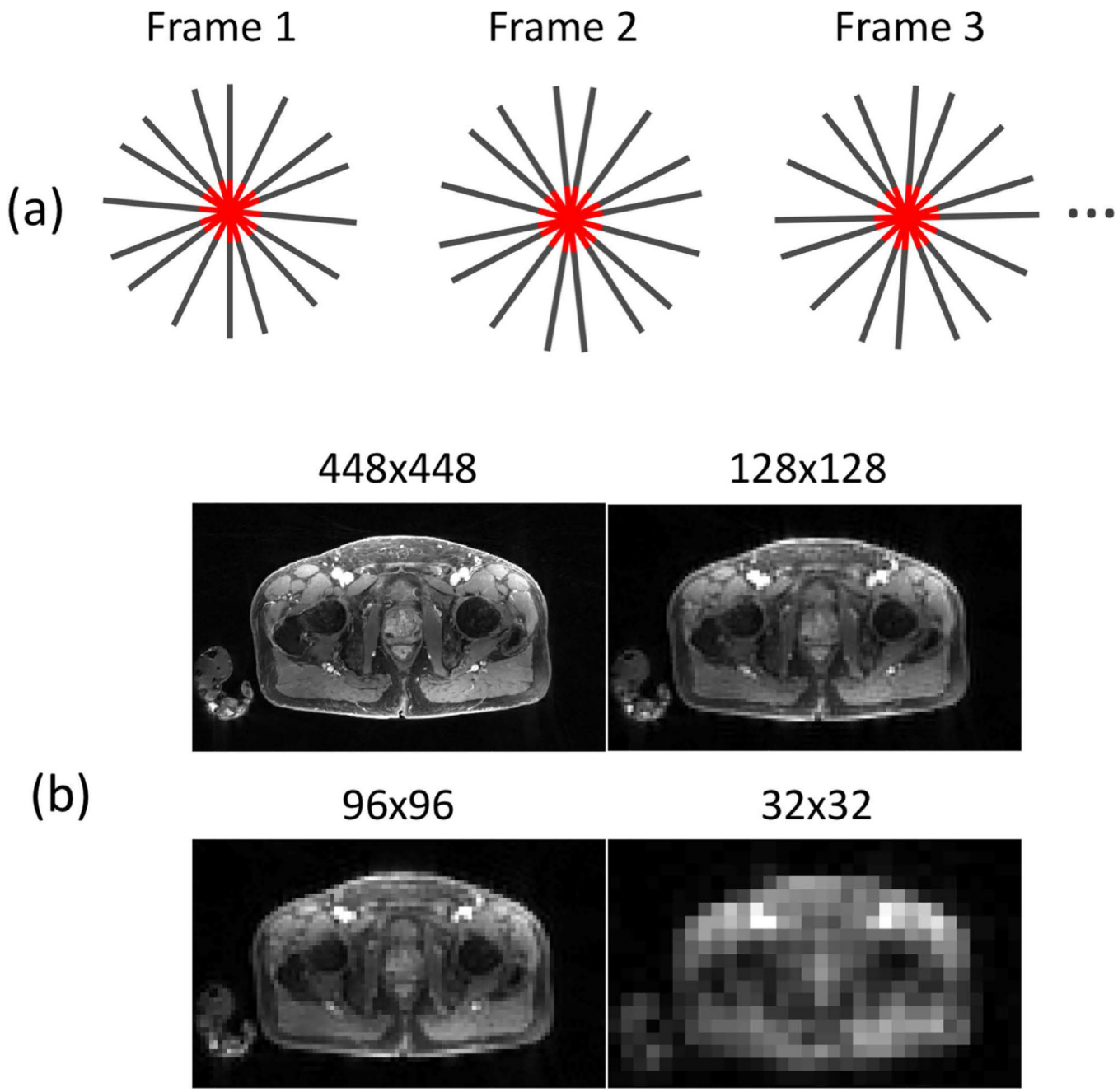

Figure 1.

(a) The unique sampling geometry of golden-angle radial sampling enables direct estimation of a temporal basis from the acquired data. Since the center of k-space (red region) is less undersampled than the periphery, a low spatial resolution dynamic image-series can be reconstructed from the low-resolution portion of the radial k-space even at high acceleration rates for estimation of the basis. (b) A fully-resolution prostate image (matrix size=448×448) with corresponding down-sampled images at different matrix sizes. Despite reduced resolution, general image content can still be visualized down to a matrix size of 96×96.

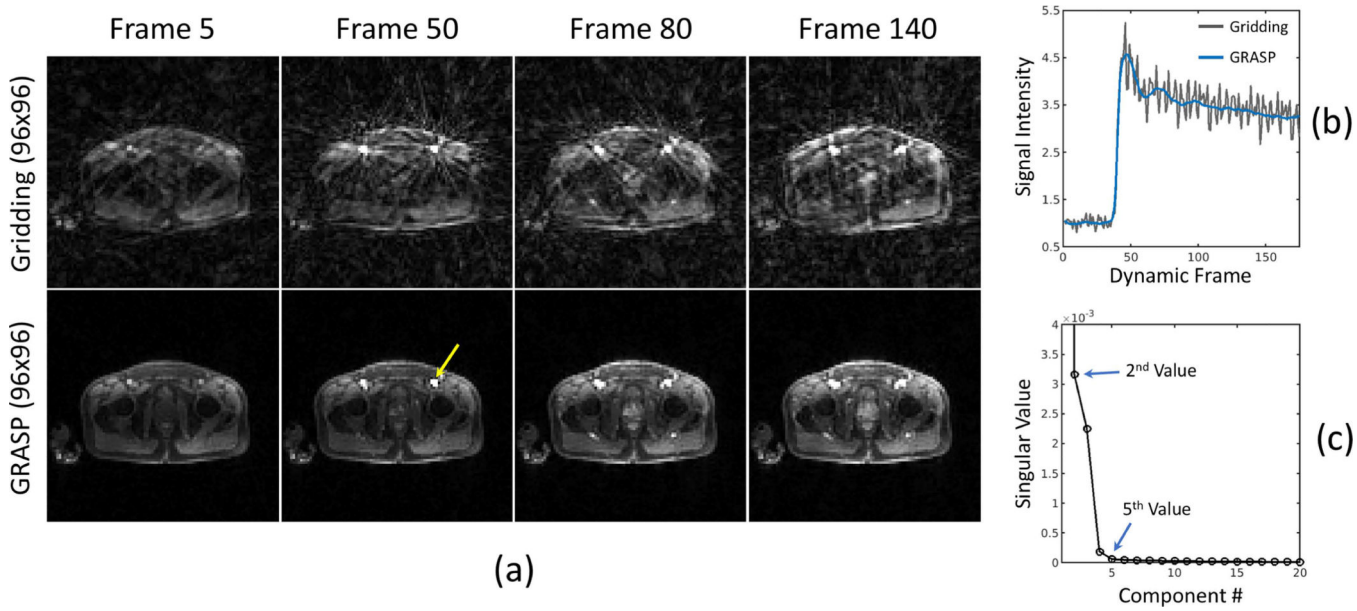

Figure 2.

(a) The low-resolution radial image-series can be reconstructed with standard GRASP even at high acceleration rates. This image-series provides full temporal information from which a temporal basis can be estimated to represent the fully-resolution images in a low-dimensional subspace. (b) Using gridding images as a reference, normalized signal-time curves from the right femoral artery (yellow arrow in the image) show good temporal fidelity of GRASP reconstruction at this low resolution. (c) Fast-decaying singular values corresponding to the low-resolution GRASP images, suggesting that the reconstructed image-series has low rank and can be represented by only a few dominant basis components.

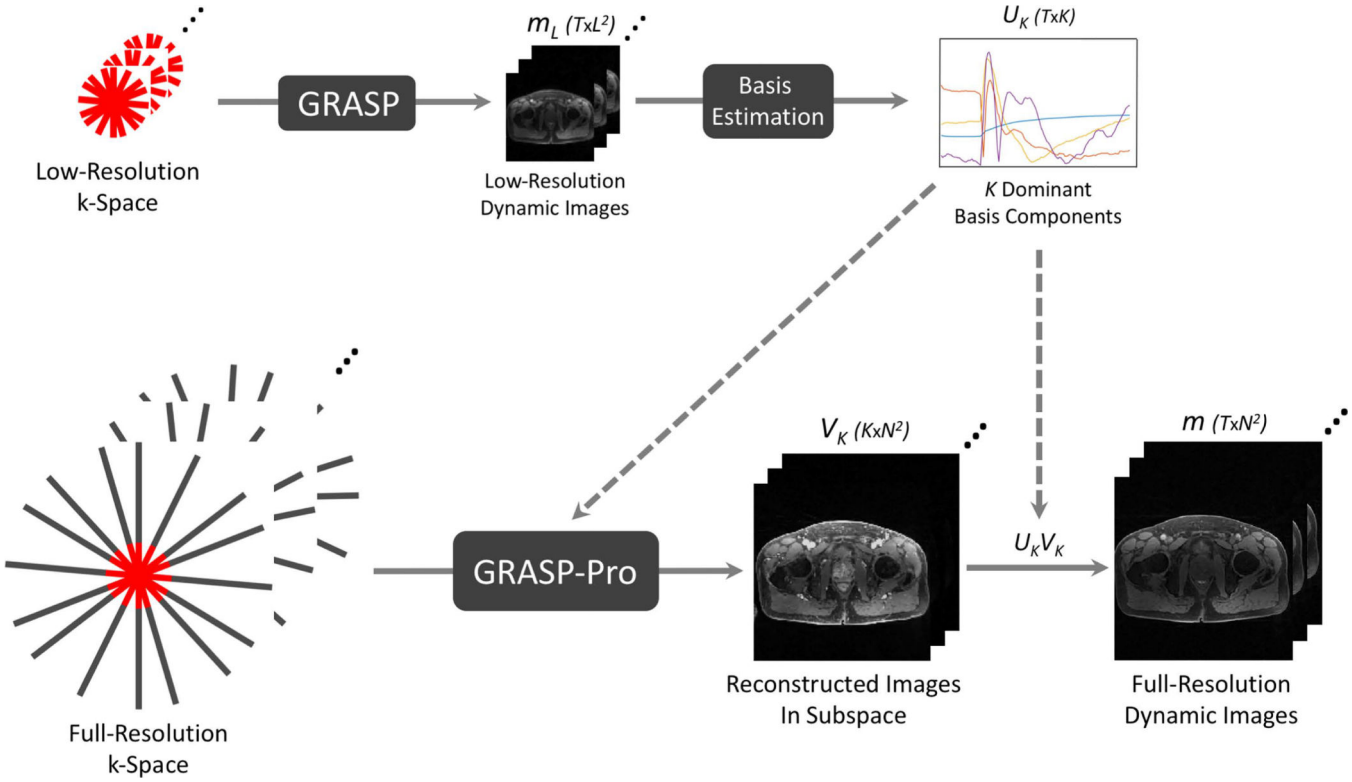

Figure 3.

The flowchart of GRASP-Pro reconstruction. As an intermediate step, standard GRASP reconstruction is performed on the low-resolution portion of the sorted radial k-space. From the reconstructed low-resolution dynamic image-series (m_L), a temporal basis is estimated, and the first dominant K basis components are kept (U_K). At the second step, GRASP-Pro is then performed on the sorted full-resolution radial k-space incorporating the pre-estimated basis (U_K) to reconstruct V_K, the coefficients to represent the fully-resolution image-series under U_K. Once V_K is reconstructed, the final images m is then computed as $U_K V_K$.

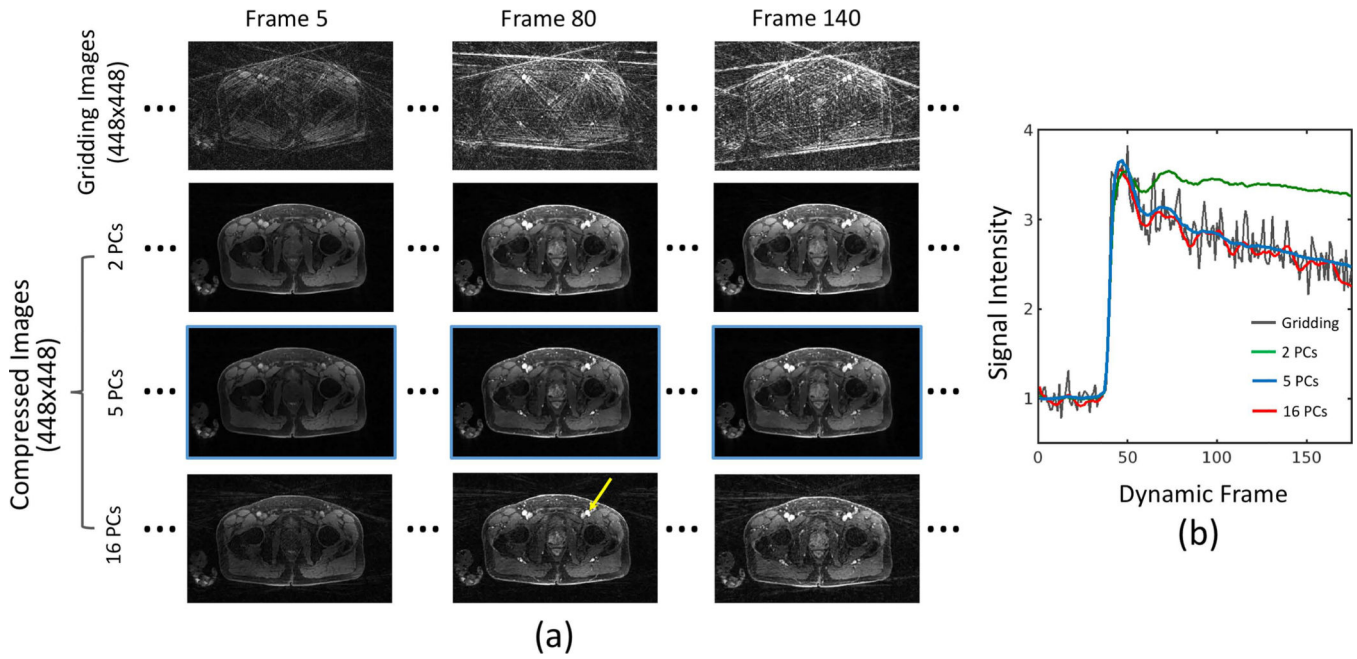

Figure 4.

Full-resolution gridding images (10 spokes each time frame) and corresponding compressed images generated from a different number of principal components (PCs) (a) and corresponding normalized signal-time profiles from the right femoral artery (b). 2 PCs generates noted temporal blurring, while 16 PCs yields residual artifacts/noise. 5 PCs were found to achieve a good balance between the compression power and the modeling error in this application.

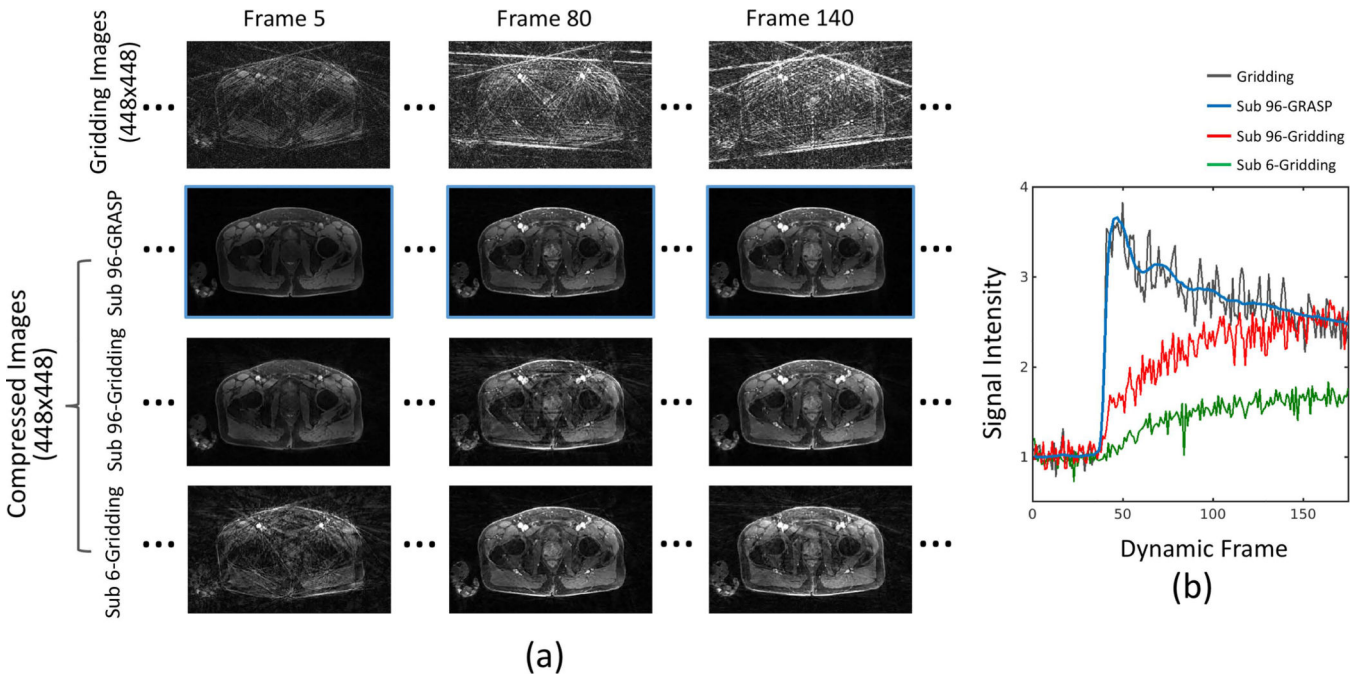

Figure 5.

(a) Full-resolution gridding images (10 spokes each time frame) and corresponding compressed images generated using basis estimated from low-resolution GRASP reconstruction (matrix size=96×96: Sub 96-GRASP) and gridding reconstruction (matrix size=96×96: Sub 96-gridding; matrix size=6×6: Sub 6-gridding). (b) Corresponding normalized signal-time profiles from the right femoral artery. Both Sub 96-gridding and Sub 6-gridding fail to produce reliable compressed images. Note that 10 spokes represent Nyquist sampling (fully sampling) for a 6×6 image.

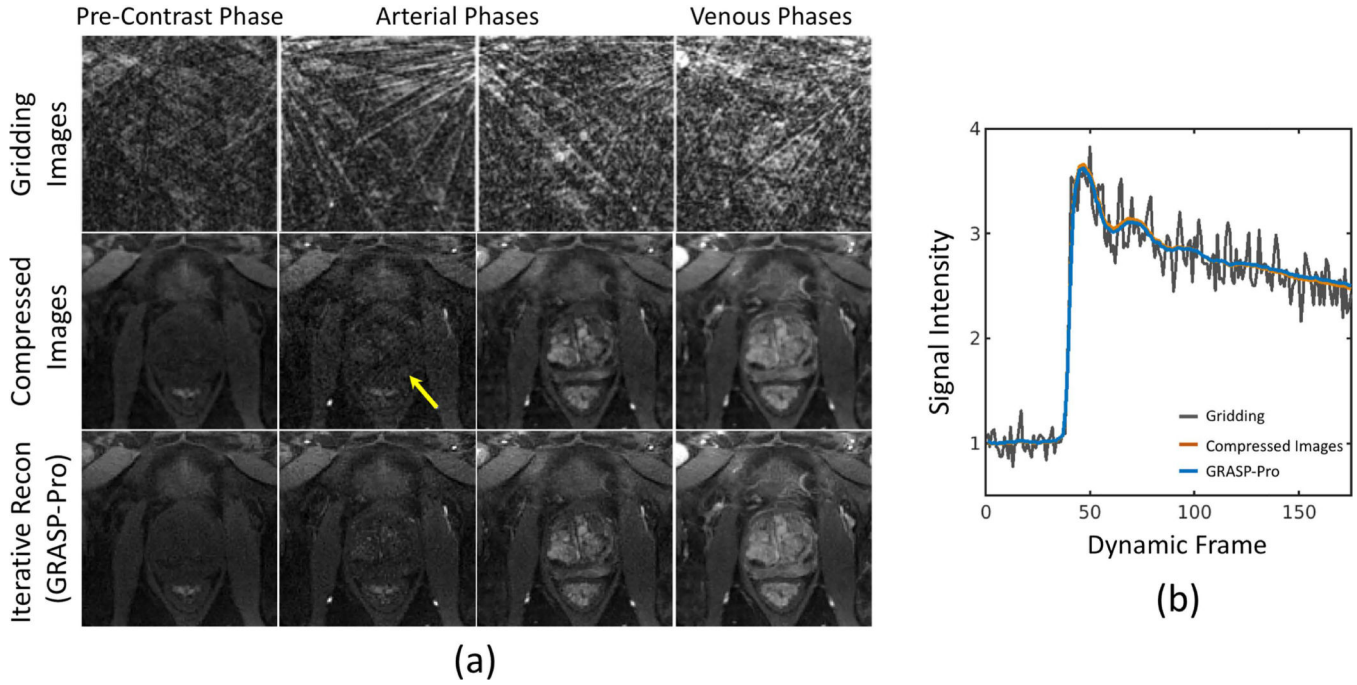

Figure 6.

(a) Comparison of gridding images with corresponding compressed images and GRASP-Pro images at different contrast phases. Compressed images, generated back from subspace with 5 PCs, have a reduced level of streaking artifacts, and GRASP-Pro further refines the dynamic images with reduced streaks and enhanced image sharpness. The yellow arrow indicates the residual streaking artifacts in the compressed images that was removed in GRASP-Pro. (b) Corresponding normalized signal-time profiles in the right femoral artery showing good temporal fidelity using gridding images as a reference.

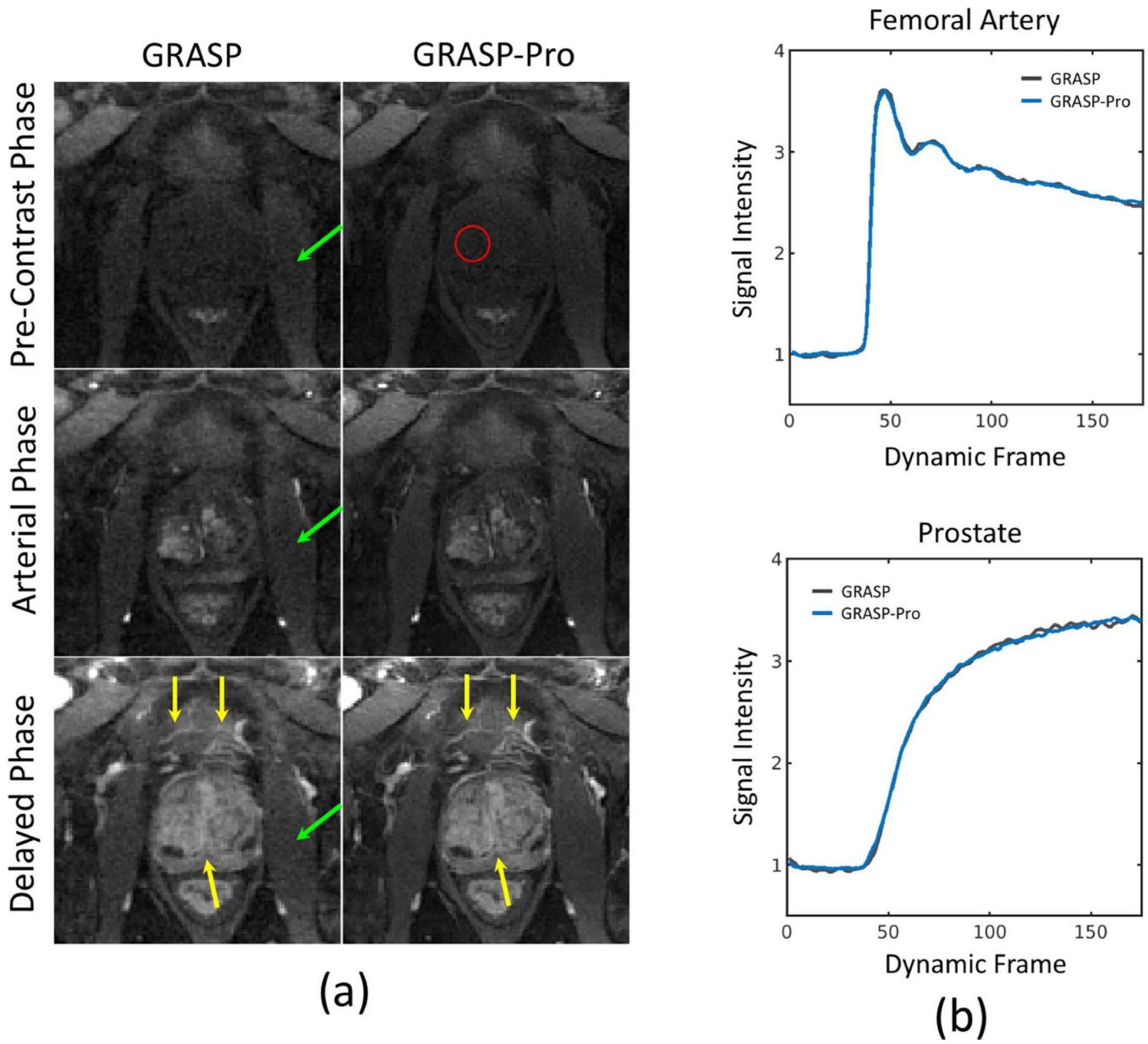

Figure 7.

Comparison of GRASP and GRASP-Pro reconstruction in one prostate patient dataset. GRASP-Pro produced cleaner images, improved sharpness, and the overall delineation of the prostate in different contrast phases.

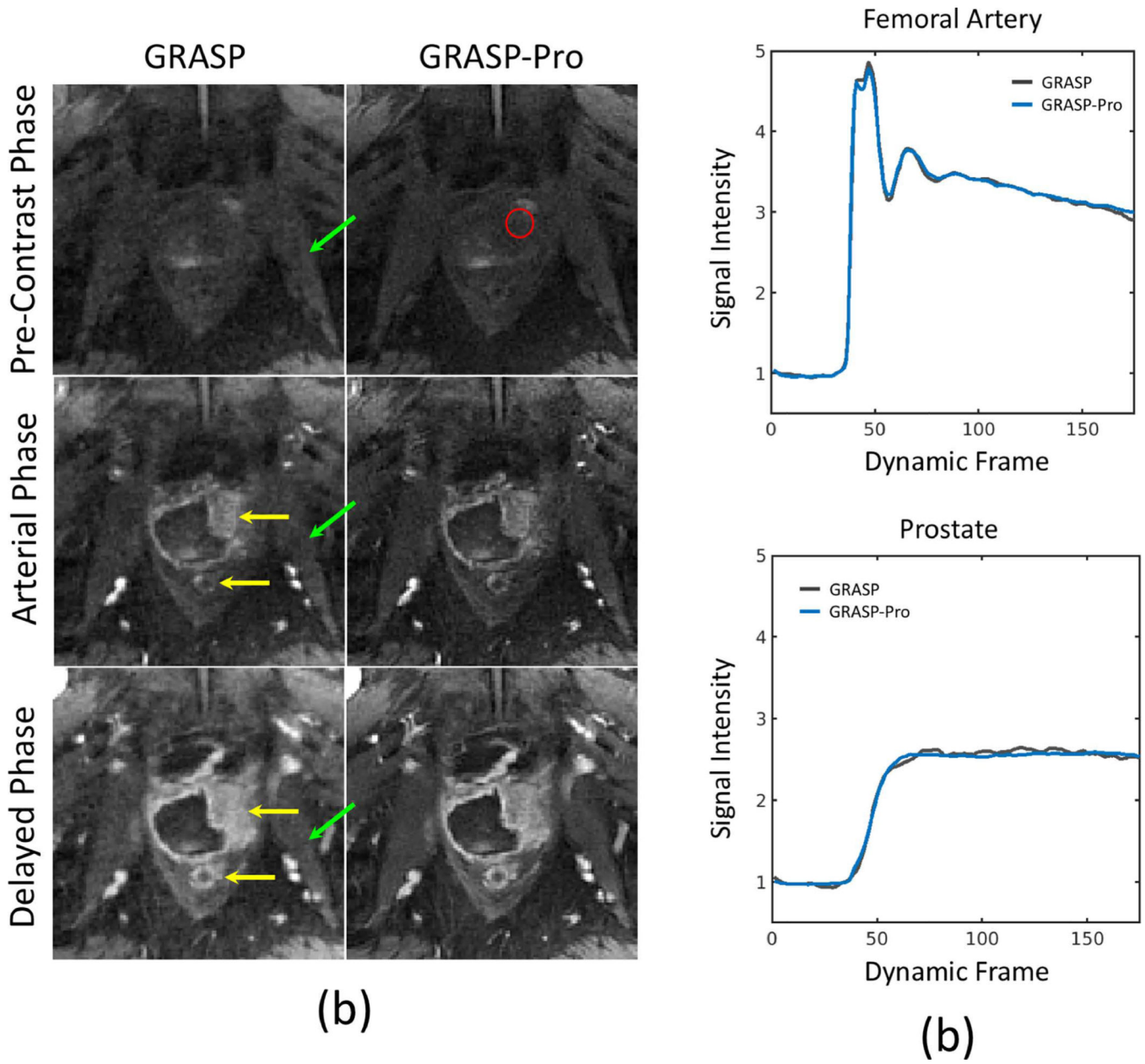

Figure 8.

Comparison of GRASP and GRASP-Pro reconstruction in another prostate patient dataset. Similar as in Figure 7, GRASP-Pro produced cleaner images, improved sharpness, and the overall delineation of the prostate in different contrast phases.

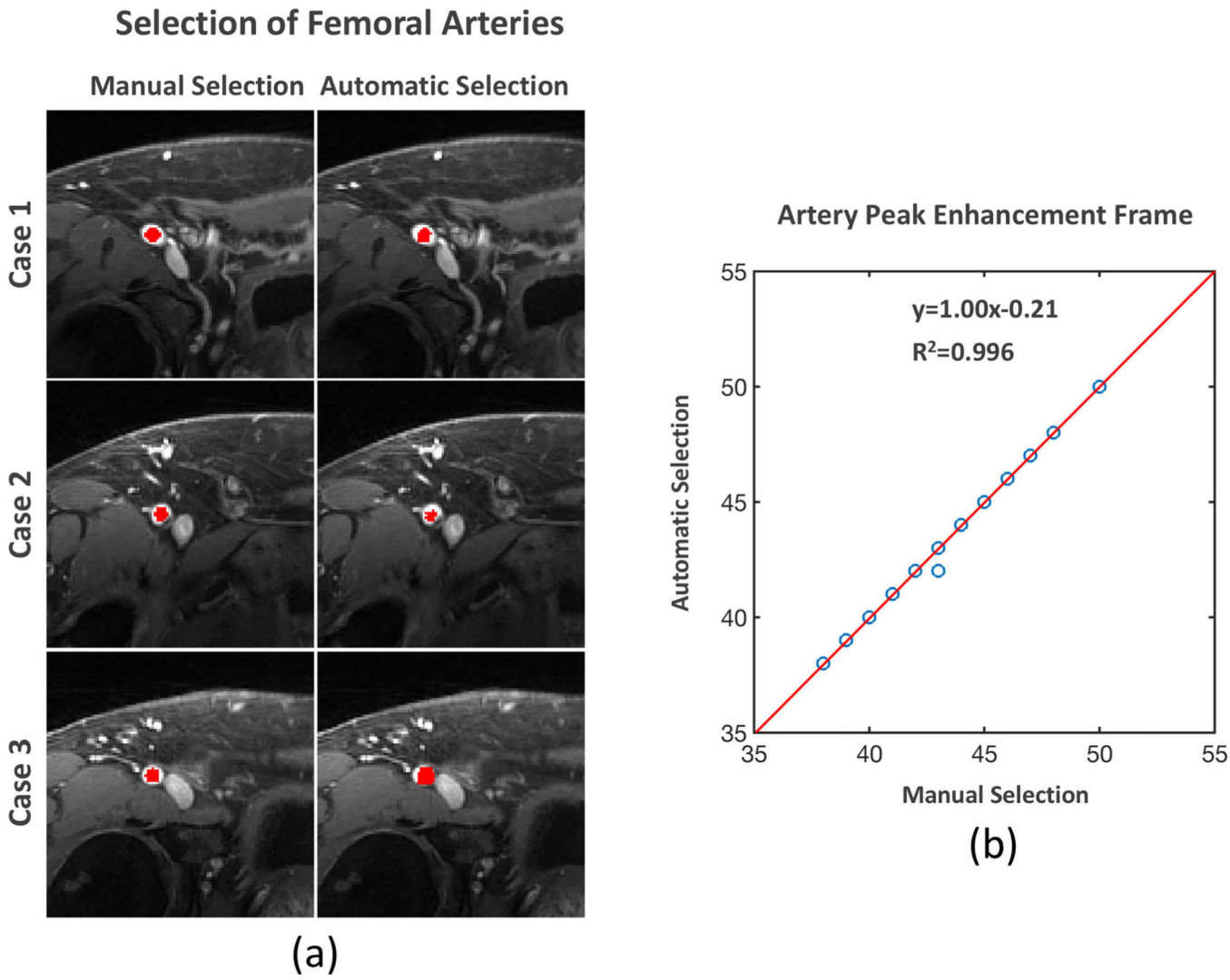

Figure 9.

(a) Comparison of manually segmentation and deep learning-based automatic segmentation of the right femoral artery in three prostate cases. Automatic segmentation could find the artery, although the performance varied from case to case. (b) The plot of linear correlation between the peak enhancement indexes obtained from automatically-generated and manually-generated contrast enhancement curves in the femoral arteries, suggesting that the network can guide the selection of desired contrast phases.

Table 1:

Visual image quality comparison between standard GRASP and GRASP-Pro for different contrast phases. The pre-contrast phase was selected at 30 seconds before the peak artery enhancement; the early arterial phase was selected at 15 seconds after the peak artery enhancement; the late arterial phase was selected at 45 seconds after the peak artery enhancement; and the delayed phase was selected at 90 seconds after the peak artery enhancement. GRASP-Pro achieved systematic improvement in all assessment categories and statistical significance was reached in all categories.

		Overall Image Quality	Sharpness of Prostatic Capsule	Streaking Artifact /Noise Level
Pre-Contrast Phase	GRASP	2.91±0.20	2.79±0.25	2.91±0.20
	GRASP-Pro	3.82±0.33$^{\neq}$	3.67±0.40$^{\neq}$	3.82±0.33$^{\neq}$
Early Arterial Phase	GRASP	3.02±0.11	3.21±0.25	3.02±0.11
	GRASP-Pro	3.98±0.11$^{\neq}$	3.98±0.11$^{\neq}$	3.98±0.11$^{\neq}$
Late Arterial Phase	GRASP	2.98±0.11	2.98±0.11	2.96±0.15
	GRASP-Pro	3.96±0.15$^{\neq}$	3.96±0.15$^{\neq}$	3.93±0.18$^{\neq}$
Delayed Phase	GRASP	3.00±0.00	3.00±0.00	3.00±0.00
	GRASP-Pro	4.00±0.00$^{\neq}$	4.00±0.00$^{\neq}$	4.00±0.00$^{\neq}$

The scoring criteria were as follows: For the overall image quality: 4=good, 3=adequate, 2=borderline, 1=non-diagnostic.

For the sharpness of prostatic capsule: 4=good, 3=adequate, 2=partially seen, 1=not seen.

For the streaking artifact/noise level: 4=none, 3=mild, 2=significant, 1= unreadable.

$^{\neq}$: The difference between GRASP-Pro and GRASP was statistically significant